Supplementary Information for "Real-Time Charge Initialization of Diamond Nitrogen-Vacancy Centers for Enhanced Spin Readout"

David A. Hopper,[1,2,*] Joseph D. Lauigan,[1,†] Tzu-Yung Huang,[1] and Lee C. Bassett[1,‡]

[1] *Quantum Engineering Laboratory, Department of Electrical and Systems Engineering, University of Pennsylvania, 200 S. 33rd St. Philadelphia, Pennsylvania, 19104, USA*

[2] *Department of Physics and Astronomy, University of Pennsylvania, 209 S. 33rd St. Philadelphia, Pennsylvania 19104, USA*

(Dated: January 6, 2020)

I. REAL-TIME CONTROL HARDWARE

Critical to this experiment is the ability for our timing electronics (AWG520, Tektronix) to be able to exit an infinite loop asynchronously and move on to a different timing sequence conditioned on an external signal. The Xilinx Artix-7 FPGA is physically interfaced with a Digital ARTY development board and perform the real-time counting and logic necessary. This platform exposes the I/O headers to communicate with the digital logic and upload the board firmware. We define the digital logic in Verilog and use the Vivado IDE to build and communicate the instructions to the board. All of our counting, both for initialization and readout, is handled by the FPGA. Given the type of counting, the FPGA either triggers an event to break out of the initialization loop or forwards the number of counts and the trial number to the DAQ via 12 digital lines after a readout has finished. The core functionality of the real-time control can be explained by three modules: control, SPAD counter, and trial counter. The control module receives information via digital lines from the AWG that governs when the FPGA should be counting, what threshold to check against, resetting registers, and whether an event should be triggered (for initialization) or if the threshold should be ignored (for readout). The SPAD counter is a 6-bit counter that records the number of rising edges coming from the SPAD and handles resetting the number of counts for a given task. The trial counter is similar to the SPAD counter, but it counts rising edges originating from the AWG. The two counters are output as a 12-bit register that the DAQ samples following the end of an experiment. This dual-counter strategy allows us to run multiple trials of a given experiment in an interleaved fashion. An example Verilog file that was used in our experiment has been posted publicly on GitHub [https://github.com/penn-qel/real-time-nv-charge-control].

II. CHARGE READOUT MODEL

We use the simplified photon distribution function originally proposed by Shields *et al.* [1], which models the observed photon distribution produced by an NV center undergoing charge readout. This model includes the effects of ionization and recombination during the

* D. A. Hopper and J. D. Lauigan contributed equally to this work.

† D. A. Hopper and J. D. Lauigan contributed equally to this work.; Present address: Quanergy Systems, 482 Mercury Dr, Sunnyvale, California 94085, USA

‡ Corresponding author. Email: lbassett@seas.upenn.edu

readout, allowing for accurate determination of the initial NV^- population. Given the NV is initially in NV^-, the photon probability distribution depends on whether there were an odd or even number of charge transitions, and is given by

$$p(n|-,\text{odd}) = \int_0^{t_R} d\tau e^{(\Gamma_{\text{Rec}}-\Gamma_{\text{Ion}})\tau-\Gamma_{\text{Rec}}t_R} \times \Gamma_{\text{Ion}} \times \text{BesselI}\left(0, 2\sqrt{\Gamma_{\text{Ion}}\Gamma_{\text{Rec}}\tau(t_R-\tau)}\right) \times \text{PoissPDF}(\gamma_-\tau + \gamma_0(t_R-\tau), n) \quad (1)$$

$$p(n|-,\text{even}) = \int_0^{t_R} d\tau e^{(\Gamma_{\text{Rec}}-\Gamma_{\text{Ion}})\tau-\Gamma_{\text{Rec}}t_R} \times \sqrt{\frac{\Gamma_{\text{Ion}}\Gamma_{\text{Rec}}\tau}{t_R-\tau}} \times \text{BesselI}\left(1, 2\sqrt{\Gamma_{\text{Ion}}\Gamma_{\text{Rec}}\tau(t_R-\tau)}\right) \times \text{PoissPDF}(\gamma_-\tau + \gamma_0(t_R-\tau), n) + e^{-\Gamma_{\text{Ion}}t_R}\text{PoissPDF}(\gamma_- t_R, n), \quad (2)$$

where γ_- (γ_0) is the photon detection rate due to NV^- (NV^0), Γ_{Ion} (Γ_{Rec}) is the ionization (recombination) rate, and t_R is the total readout duration PoissPDF is the probability density function of a Poisson distribution and is given by

$$\text{PoissPDF}(\lambda, n) = \frac{\lambda^n e^{-\lambda}}{n!}, \quad (3)$$

where λ is the mean number of detected photons, and n is the number of photons detected. BesselI is a modified Bessel function of the first kind and is given by

$$\text{BesselI}(\nu, z) = \left(\frac{1}{2}z\right)^\nu \sum_{k=0}^{\infty} \frac{\left(\frac{1}{4}z^2\right)^k}{k!\Gamma(\nu+k+1)}. \quad (4)$$

The full photon distribution given starting in NV^- is

$$p(n|-) = \frac{1}{2}(p(n|-,\text{odd}) + p(n|-,\text{even})). \quad (5)$$

To get the equivalent expression for NV^0, simply swap the ionization and recombination rates as well as the photon rates ($\Gamma_{\text{Ion}} \leftrightarrow \Gamma_{\text{Rec}}$ and $\gamma_- \leftrightarrow \gamma_0$) in Eqs. 1 and 2. A general mixture of the two charge states is given by

$$p(n) = P_- p(n|-) + (1-P_-)p(n|0), \quad (6)$$

where P_- is the initial population of NV^- prior to the start of readout. In this work, we evaluate Eq. 6 numerically in MATLAB and either fit to measured distributions or simulate the expected photon distribution for a given choice of rates and readout duration.

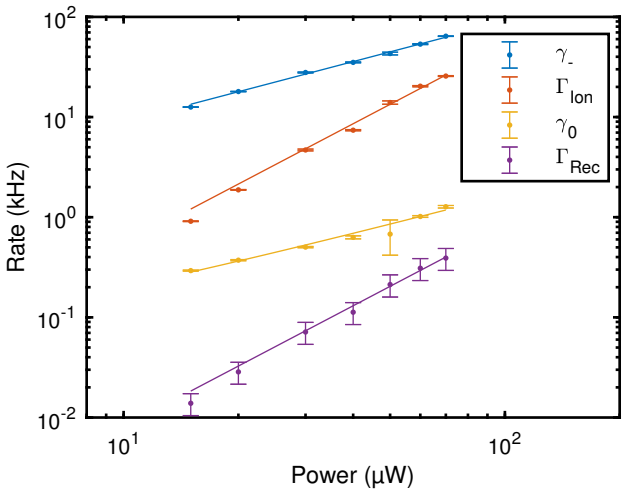

SFIG. 1. Red Charge Dynamics Calibration. The four measured rates and their associated power-dependence fits are presented.

III. RED CHARGE DYNAMICS CALIBRATION

To calibrate the red charge dynamics, we fit measured photon distributions to the model previously described for different red powers. The readout duration is chosen such that $t_R > {\Gamma_{\text{Ion}}}^{-1}$, allowing for the effects of ionization to be observed. The readout duration does not need to be longer than the recombination rate, as it is given by

$$\Gamma_{\text{rec}} = \frac{P_-}{1 - P_-}\Gamma_{\text{ion}}. \tag{7}$$

Due to the small recombination rate under red illumination, the steady state NV^- population is $P_- = 1.15 \pm 0.07\%$. This complicates measuring the charge dynamics as it is difficult to observe NV^- fluorescence during continuous red illumination. To overcome this, we implement a pump-probe scheme to determine the red charge dynamics. A 10 µs green charge pump is followed by a variable power and duration red charge probe during which the number of photons are counted. This increases the average initial NV^- population to $\approx 75\%$. The results of the charge dynamics calibration are presented in SFigure 1. We fit all of the rates to their unsaturated form [2] due to the maximum power being well below

Parameter	Value
C_-	0.895 ± 0.027 kHz µW^{-1}
C_0	0.0163 ± 0.0023 kHz µW^{-1}
D	0.039 ± 0.067 kHz
C_{Ion}	5.36 ± 0.27 Hz µW^{-2}
C_{Rec}	0.082 ± 0.0041 Hz µW^{-2}

TABLE I. Fit results for the charge dynamics calibration.

saturation. The power-dependencies for the rates are as follows

$$\gamma_- = C_- P \tag{8}$$

$$\gamma_0 = C_0 P + D \tag{9}$$

$$\Gamma_{\mathrm{Ion}} = C_{\mathrm{Ion}} P^2 \tag{10}$$

$$\Gamma_{\mathrm{Rec}} = C_{\mathrm{Rec}} P^2, \tag{11}$$

where C_s is the rate scaling term for the s process and D is the dark count rate. The fit parameters are presented in Table I. The agreement of the data with the fit model further supports the use of the unsaturated rate dependencies.

IV. SPIN PROPERTIES FOLLOWING REAL-TIME INITIALIZATION

The ground state spin properties were measured for both the steady state and real-time initialization protocols. First, we performed a Ramsey measurement on the NV center spin for both initialization techniques and measured the resulting spin population with traditional PL readout. The $\pi/2$ pulses were detuned from resonance by 5 MHz to simplify the free evolution dynamics with the coupled ^{14}N nuclear spin. The data were fit to the model

$$S = C + A * e^{-(\tau/T_2^*)^2} \sum_{k=-1}^{1} \cos\left(2\pi(\delta - kA_{||}) + \phi\right), \tag{12}$$

where C is the dephased signal, A is the amplitude of the signal, τ is the evolution time, T_2^* is the inhomogenous dephasing timescale in µs, δ is the detuning from resonance in MHz, $A_{||}$ is the parallel hyperfine coupling due to ^{14}N in MHz, and ϕ is a phase offset in radians. The data and fit results are depicted in SFig. 2(a, b) for the steady state and real-time

initialization protocols, respectively. We find a steady state $T_2^{*,SS} = 1.92 \pm 0.08$µs and a real-time $T_2^{*,RT} = 2.24 \pm 0.10$µs, which corresponds to a 16% increase in spin dephasing time scale with the real-time initialization.

We then performed a Hahn-echo measurement for both of the initialization techniques. We initially identified the revivals due to the ^{13}C spin bath and then measured the amplitudes of these revivals. The final $\pi/2$ was applied around the $+X$ and $-X$ axes to allow for a differential signal, which can be seen in SFig. 2(c,d) for the steady state and real-time protocols, respectively. The resulting data are fit to the model

$$S = C + Ae^{-(\tau/T_2)^n}, \tag{13}$$

where C is the offset, A is the amplitude, T_2 is the echo coherence, and n is a freely varying parameter for the stretched exponential [1]. The steady state initialization results in a coherence time of $T_2^{SS} = 830 \pm 28$ µs and $n = 2.98 \pm 0.42$. The real time initialization results in a coherence time of $T_2^{RT} = 852 \pm 81$ µs and $n = 2.85 \pm 1.03$.

We also measured the spin relaxation time for both initialization techniques. To do this, we first initialize into the $m_s = 0$ projection and then record the SCC signal for various wait times. The data is presented in SFigure 2(e, f) for the steady state and real-time initialization protocols, respectively. The data in both cases is fit to a single exponential, which results in a spin relaxation time of $T_1^{SS} = 5.6 \pm 1.2$ms and $T_1^{RT} = 5.3 \pm 0.9$ms for the steady state and real-time protocols, respectively. Thus, there is no measurable difference between the two techniques.

V. SPIN READOUT PARAMETER OPTIMIZATION

Both spin readout methods are calibrated to optimize their SNR to ensure that we are fairly comparing their performance. The calibration of traditional PL readout is presented in SFigure 3. We take time-tagged measurements of the transient fluorescence response to different 532 nm illumination intensities [SFig. 3(d)] for both initialization techniques. A few powers above and below the saturation power were chosen; note that we observed the quenching of fluorescence at higher powers [SFig. 3(b)]. From these time-traces, we can calculate the average number of detected photons for various integration windows and powers and find the global optimum. We present how the optimum readout duration [SFig. 3(c)]

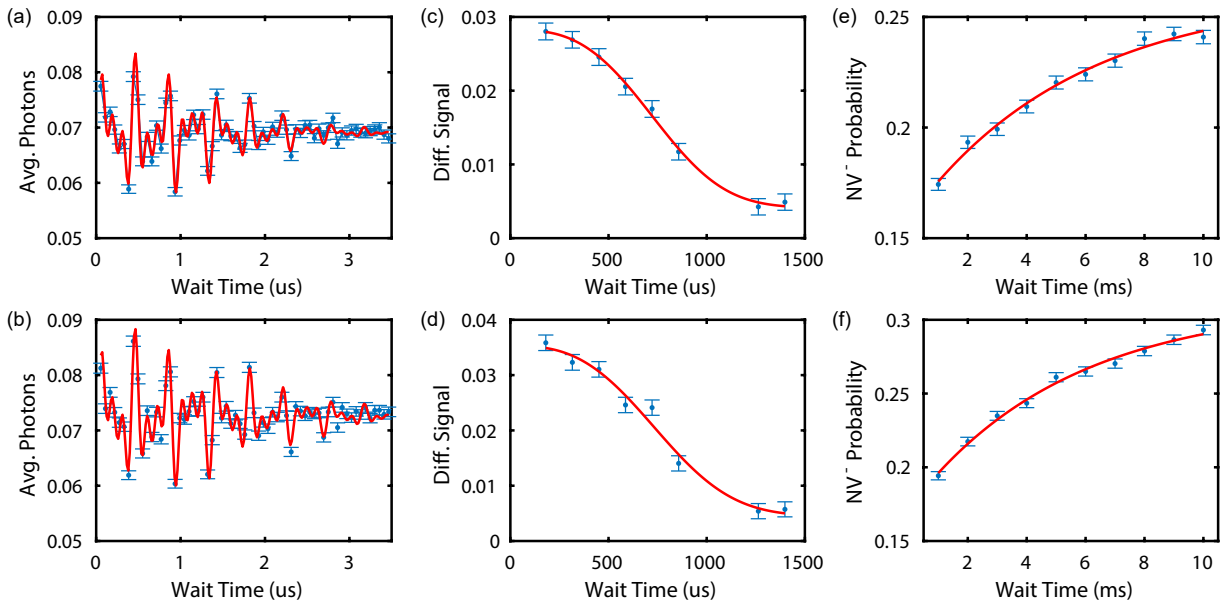

SFIG. 2. Spin Property Comparison. Measurements of T_2^* (a, b), T_2 (c, d), and T_1 (e, f) for the steady state and real-time initialization protocols, respectively.

and the optimum SNR [SFig. 3(d)] vary for different powers. We find that both initialization techniques require the same readout duration and power, and find a strong quenching of the SNR for higher powers which coincides with the quenched saturation fluorescence, suggesting that a careful calibration of PL readout parameters is necessary when the NV is efficiently pumped.

For spin-to-charge conversion (SCC), we follow a similar calibration scheme laid out in Supplemental Reference [1], in which we sweep the durations of the orange shelf and red ionization pulse independently. The approximate optimal shelf duration and power can be found by looking for the maximum instantaneous contrast between the $m_s = 0$ and $m_s = \pm 1$ states through a transient measurement [such as those in SFIG. 3(a)]. This initial calibration helps to reduce the large parameter space of the SCC readout properties. For a given measurement sweeping over shelf or ionization duration, we simultaneously fit all of the charge readout distributions to the same underlying rates, but allow the NV^- population for each spin and parameter to vary, thus reducing the covariance between NV^- population and the ionization rate. The results of the fitted NV^- populations for these measurements are in SFig. 4. We find an optimum ionization pulse settings of 20 ns and 40 mW and a shelf settings of 30 ns and 500 µW. This produces a single-shot SNR=0.5 with an initial NV^-

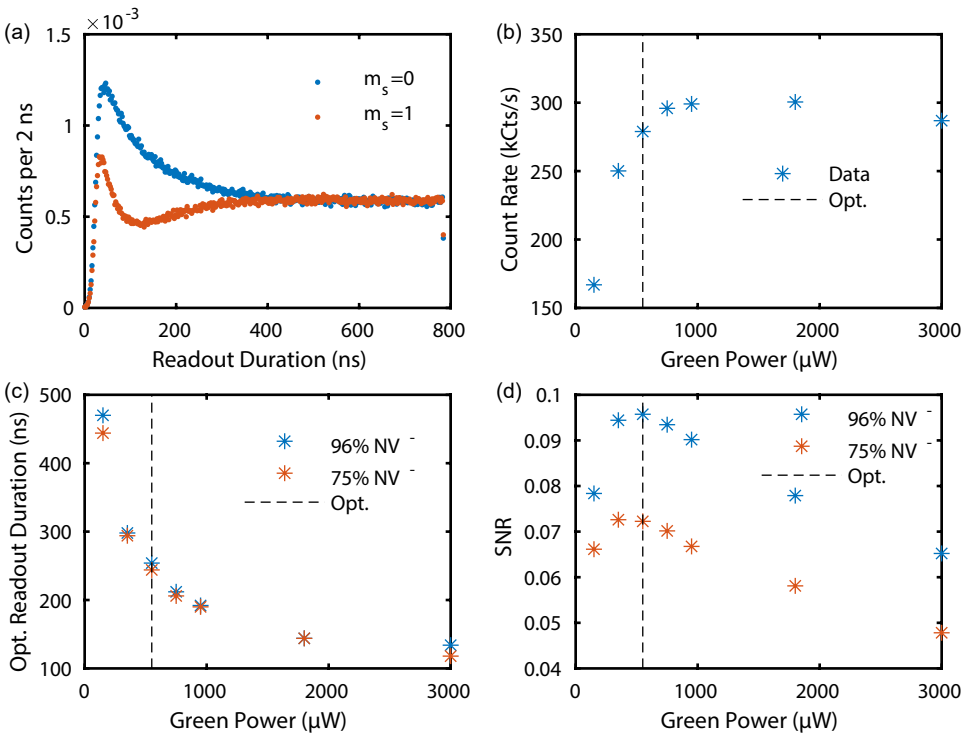

SFIG. 3. Traditional PL Readout Calibration (a) Example transient response due to the two spin states with 532 nm illumination. (b) The steady state count rate for different 532 nm powers. (c,d) The optimum spin readout SNR and the corresponding power and readout duration as well as how they vary for different powers.

fidelity of 98%.

VI. CALIBRATING SPIN SNR

The measured observables for different initialization fidelities and both readout techniques are presented in SFig. 5. For both readout techniques, the data are fit to Equation 6 in the main text, where we fix the error term to be the same for both initial spin states. To be in line with the literature, we set $S = \alpha$ when our signal consists of average detected photons, and $S = \beta$ when our signal is the probability of detecting NV^-. For PL readout [SFig. 5(a)], the fitting yields $\langle \tilde{\alpha}_0' \rangle = 9.664(1) \times 10^{-2}$ photons, $\langle \tilde{\alpha}_1' \rangle = 5.254(1) \times 10^{-2}$ photons, and $\langle \alpha_\epsilon \rangle = 2.703(3) \times 10^{-6}$ photons. For SCC readout [SFig. 5(b)], the fitting yields $\langle \tilde{\beta}_0' \rangle = 0.1581(1)$ %, $\langle \tilde{\beta}_1' \rangle = 0.4778(2)$ %, and $\langle \beta_\epsilon \rangle = 0.0530(4)$ %.

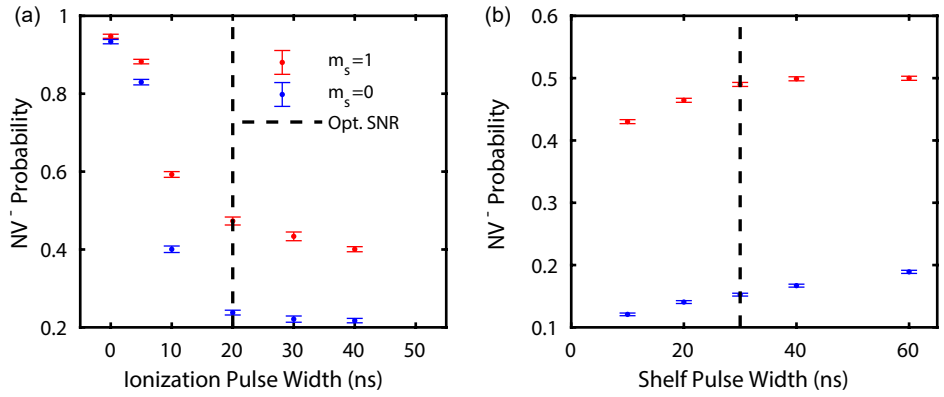

SFIG. 4. SCC Readout Calibration (a) NV^- population for various ionization pulse widths (a) and shelf widths (b) for both spin states. The dashed black line signifies the optimal parameters for maximized single-shot SNR.

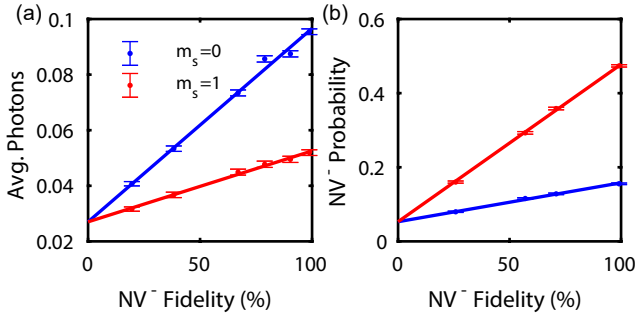

SFIG. 5. Fitting to spin observables (a) Average detected photons for both spin states and various initial NV^- fidelities. (b) NV^- probability following SCC for both spin states and various initial NV^- fidelities. Solid lines are fits to Eqn. 6 in the main text where the error term is held constant between the two lines.

VII. SPIN POLARIZATION ESTIMATION

The ground state spin polarization of the NV center can be estimated by observing the relative amplitudes of the bi-exponential decay of a pulsed lifetime measurement [1, 3, 4]. By performing a fit to the lifetime response for both the optically polarized state, as well as after a calibrated π-pulse, one can estimate the initial $m_s = 0$ population, assuming there is negligible radiative spin-mixing in the triplet manifold. However, to accurately fit the lifetime response, one must take into account the other spin projection ($m_s = -1$ in our case), as well as pulse errors that manifest from the ^{14}N hyperfine coupling. We now write

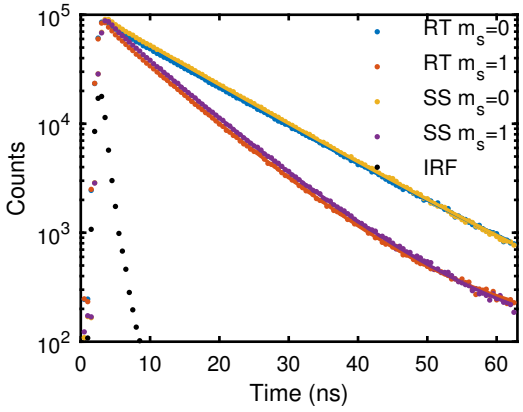

SFIG. 6. Lifetime Measurement of Spin Polarization. Transient response to a $< 2.5\,\text{ns}$ red pulse for both the $m_s = 0, 1$ spin states and the real-time (RT) and steady state (SS) initialization protocols. The measured instrument response function (IRF) is also displayed.

down the three spin projection populations before

$$\begin{pmatrix} p^b_{-1} \\ p^b_{+1} \\ p^b_0 \end{pmatrix} = \begin{pmatrix} \frac{1-p_0}{2} \\ \frac{1-p_0}{2} \\ p_0 \end{pmatrix}, \tag{14}$$

and after the inversion pulse

$$\begin{pmatrix} p^a_{-1} \\ p^a_{+1} \\ p^a_0 \end{pmatrix} = \begin{pmatrix} \frac{1-p_0}{2} \\ \frac{1-p_0}{2} \times (1 - F_\pi) + p_0 \times F_\pi \\ p_0 \times (1 - F_\pi) + \frac{1-p_0}{2} \times F_\pi \end{pmatrix}, \tag{15}$$

where F_π is the fidelity of the π-pulse, which for this measurement with a Rabi driving frequency of $\sim 5\,\text{MHz}$ is approximated to be 88%. The transient fluorescence response is then given by

$$f(t) = A_i \left(p^i_0 e^{-\gamma_0 t} + (p^i_{+1} + p^i_{-1}) e^{-\gamma_1 t} \right) + C, \tag{16}$$

where A_i is an overall amplitude, $i = a, b$ represents whether this was after or before the inversion pulse, and γ_i is the excited state decay rate for the magnitude of the spin projection i, and C is a background term.

To perform the lifetime measurement, we initialize the NV center (either with the real-time or steady state protocol) and then measure the transient fluorescence response following

a short excitation pulse with the red laser. The red laser can produce a pulse that is $\sim 2\,\mathrm{ns}$ in duration. The instrument response function (IRF) for this can be seen in SFig. 6. The data for both spin states and initialization protocols is presented in SFig.6. We simulatenously fit Equation 16, convolved with the IRF, to the before and after inversion pulse data sets. This helps reduce covariance between the excited state decay rates and the relative amplitudes and has been utilized in the literature [3]. We determine the excited state lifetimes to be $\gamma_0^{-1} = 12.50 \pm 0.02\,\mathrm{ns}$, and $\gamma_1^{-1} = 7.48 \pm 0.02\,\mathrm{ns}$. The spin polarization in $m_s = 0$ (p_0) is found to be $91.5 \pm 0.7\%$ and $94.4 \pm 0.7\%$ for the steady state and real-time initialization techniques, respectively.

It should be noted that since our excitation pulse is of similar magnitude to the fastest decay rate ($\gamma_1^{-1} = 7.5\,\mathrm{ns}$), the spin polarization measured for the steady state technique may be slightly lower in actuality than measured, as the optical pumping process has begun during the non-instantaneous rise and fall time. Nonetheless, we still measure a difference in the spin polarizations for the two techniques, which agrees with the independent observation of the SNR differences mentioned in the main text.

VIII. SPEEDUP AND PHOTON COLLECTION EFFICIENCY

The model parameters are scaled as follows. First, the PL SNR is scaled by the square root of the ratio of the saturated count rates

$$\mathrm{SNR}_{\mathrm{new}} = \sqrt{\frac{C_{\mathrm{New}}}{C_{\mathrm{Ref.}}}}\mathrm{SNR}_{\mathrm{Ref.}}, \tag{17}$$

where C_{New} is the new saturated count rate to be studied, $C_{\mathrm{Ref.}} = 300\,\mathrm{kCts/s}$ is the saturated count rate in this study, and $\mathrm{SNR}_{\mathrm{Ref.}}$ is the calibrated PL readout SNR in this study. This scaling is performed for both the baseline technique, SSI with PL readout, as well as RTI with PL readout. Second, the initialization and charge readout processes are modified by scaling the NV^- emission rate, given by

$$\gamma_-^{\mathrm{New}} = \frac{C_{\mathrm{New}}}{C_{\mathrm{Ref.}}}\gamma_-^{\mathrm{Ref.}}, \tag{18}$$

where $\gamma_-^{\mathrm{Ref.}}$ is the NV^- emission rate from Eq. 8. The other charge-related rates and the power scaling are unchanged.

The modeled speedup curves for saturated 532 nm count rates of 60 kCts/s, 125 kCts/s, 600 kCts/s, and 900 kCts/s are presented in SFig. 7. The break-even time depicted in the

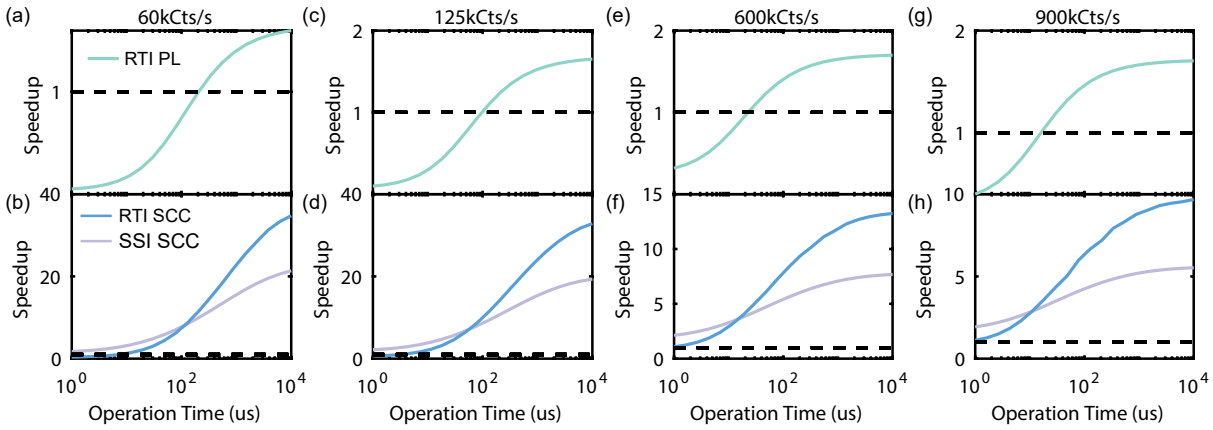

SFIG. 7. Speedup and Photon Collection Efficiency. The predicted speedup of the initialization and readout techniques discussed in the main text assuming saturated count rates of 60 kCts/s (a, b), 125 kCts/s (c, d), 600 kCts/s (e, f), and 900 kCts/s (g, h) under continuous 532 nm illumination. The dashed black line denotes the break-even situation (Speedup=1).

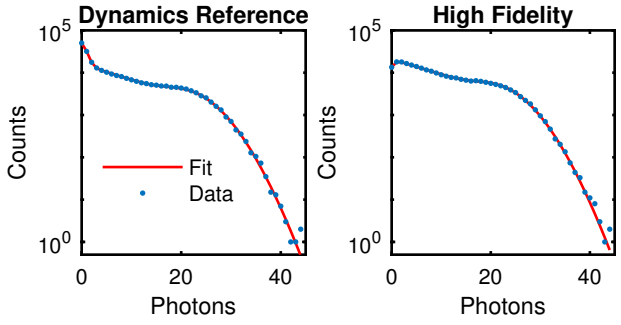

SFIG. 8. Measuring High Fidelity Initialization (a) The readout distribution resulting from a $73.3 \pm 0.2\%$ NV^- population and corresponding fit. (b) The readout distribution resulting from a $99.4 \pm 0.1\%$ NV^- population. The two curves are jointly fit to a model that fixes the charge dynamics but allows the initial NV^- population to vary.

main text is the operation time at which the spin readout efficiency for a given readout technique is equal for both SSI and RTI.

IX. HIGH FIDELITY INITIALIZATION

High fidelity initialization can be achieved by increasing the threshold condition with similar probe power and durations that were presented in the main text. To measure a

high fidelity initialization attempt, we perform two interleaved measurements. The first is a reference measurement where we measure the charge readout distribution due to a typical 532 nm pump pulse, the second is the real-time initialization with charge probe settings of $P_{probe} = 6\,\mu W$, $\tau_{probe} = 9\,\mu s$, and a threshold increased to $\nu = 2$. We simultaneously fit to both the reference and high fidelity charge readout distributions where we fix the system dynamics between the two measurements $(\gamma_0, \gamma_-, \Gamma_{Ion})$ and allow the NV^- populations to vary. The elevated threshold has the effect of drastically increasing the average attempts but purifying the initial state. We repeat the reference and real-time initialization measurement for 250,000 repeats, each; the results of this measurement are in SFigure 8. We determinee that the NV can be initialized into $F_{NV^-} = 99.4 \pm 0.1\%$ with an average time-to-initialize of 7 ms. The maximum fidelity attainable with a threshold of 1 is $98.6 \pm 0.2\%$, which corresponds to an initialization error rate of 1.4%, while a threshold of 2 results in an initialization error rate of 0.6% which leads to a factor of 2.5 reduction in error rate. In this regime, the initialization fidelity is limited by the signal-to-background ratio of the charge readout process.

[1] B. J. Shields, Q. P. Unterreithmeier, N. P. de Leon, H. Park, and M. D. Lukin, Efficient readout of a single spin state in diamond via spin-to-charge conversion, Phys. Rev. Lett. **114**, 136402 (2015).

[2] N. Aslam, G. Waldherr, P. Neumann, F. Jelezko, and J. Wrachtrup, Photo-induced ionization dynamics of the nitrogen vacancy defect in diamond investigated by single-shot charge state detection, New J. Phys. **15**, 13064 (2013).

[3] G. D. Fuchs, V. V. Dobrovitski, D. M. Toyli, F. J. Heremans, C. D. Weis, T. Schenkel, and D. D. Awschalom, Excited-state spin coherence of a single nitrogen-vacancy centre in diamond, Nat. Phys. **6**, 668 (2010).

[4] L. Robledo, H. Bernien, T. V. D. Sar, R. Hanson, T. van der Sar, and R. Hanson, Spin dynamics in the optical cycle of single nitrogen-vacancy centres in diamond, New J. Phys. **13**, 25013 (2011).